International Journal of Networking and Computing – www.ijnc.org, ISSN 2185-2847
Volume 8, Number 2, pages 351–366, July 2018

Moving target approach for wind-aware flight path generation

Marius Klein, Andreas Klos, Jörg Lenhardt, Wolfram Schiffmann
Faculty of Mathematics and Computer Science
FernUniversität in Hagen, Germany
Marius.Klein,Andreas.Klos,Joerg.Lenhardt,Wolfram.Schiffmann@FernUni-Hagen.de

Received: February 1, 2018
Revised: May 4, 2018
Accepted: June 11, 2018
Communicated by Susumu Matsumae

Abstract

A total loss of thrust poses a major hazard to passengers and aircrafts. In such situations, the pilot is forced to perform an emergency landing by fast and intuitive decisions. During the manoeuvre, the potential energy of the aircrafts altitude is converted into the kinetic energy to move a certain distance over ground. This may enable the aircraft to reach a suitable landing field at a proper altitude. In this paper, we introduce an emergency landing assistant which calculates the flight path from a start to a target position with uniform computational complexity. The main objective is to support the pilot and accelerate the decision-making process. Our path computations take a constant wind into account by moving the target runway contrary to the wind direction. The results have shown that even with the restriction of co-rotating circles a high percentage of valid flight paths can be found. Furthermore, for most of the considered start configurations more than one feasible flight path can be discovered.

1 Introduction

Forced landings can be caused by total or partial engine-failures, fire or smoke on board etc. In this study, we consider aircrafts with a total loss of thrust caused by an engine-failure. In such situations, the pilot is forced to conduct an emergency landing. Fast, intuitive, and proper decisions determine the viability of the passengers and the aircraft. The support of the pilot during such extreme situations is considered as major issue. Moreover, the importance of such an Emergency Landing Assistant (ELA) gained much attention because of the US Airways Flight 1549 in 2009. Short after take-off a bird-strike occurred and both engines of the Airbus A320 failed so that the pilot was forced to perform an emergency landing. In this situation, it is desirable to have a supporting assistant system which takes over the guidance to the most suitable of runways within reach.

In this study, we present ELA which is capable to compute the flight path from the current configuration of the aircraft (position, heading, speed) to an emergency landing field. Thereby, a database with possible emergency landing fields is assumed to be available. These are published airfields with paved runways in the best case. The corresponding geodata of those airfields is available worldwide. In another paper of the work group we will present how to identify those emergency landing fields [1].

Frequently, Dubins curves are used to calculate the path between two configurations of a kinematic model. Dubins curves [2] were introduced in 1957 and are used for the computation of the shortest, possible path between two car configurations. To compute flight paths for aircrafts these originally two-dimensional approaches have been extended by the third dimension in recent years [3].

During the glide along the flight path the excess altitude is used to compensate the missing thrust in order to reach an emergency landing field. Simultaneously, most of the excess altitude should be consumed on the glide path so that the aircraft reaches the beginning of the emergency landing field at an appropriate altitude of a few meters above ground and with a suitable landing configuration (air speed and runway heading).

Unfortunately, previous research on Dubins curves was restricted to windless situations. Obviously, the influence of the wind has to be considered, especially, if the wind contributes to a non negligible share of the aircraft's velocity. In order to take the wind into account, methods have been used that observe the aircraft from the earth (frame) which causes trochoidal curves [4]. Thereby, a start trochoid is applied at the emergency configuration. At the runway configuration a final trochoid is fitted. Both trochoids have to be connected by a tangent. However, the trochoid method has three serious disadvantages: First, the altitude loss during the gliding path can only be adopted by the variation of the trochoid radii and/or the number of turns. Second, the calculation of the tangent is complex and only an approximated solution can be found. Third, it is restricted to a two circle approach and uniform wind conditions during the glide.

In this paper, we address the wind problem by an elementary but efficient solution that can be used with any type of approach path which offers more flexibility, even though the aircraft is gliding through layers with changing wind patterns. Nevertheless, in this paper we only consider a constant wind vector.

The basic idea of our technique is to perform the calculations in the wind frame and transform the resulting flight path back to the earth frame. This method avoids the complicated computations of fitting the trochoids to the start and final configurations. Instead we move the destination in the wind frame (e. g. runway threshold) opposite to the wind direction. The subsequent path calculations are performed as in the windless case and thus the complexity of the computation can be reduced dramatically.

The wind and earth frame are congruent in the windless case. Under the influence of wind, the frame moves opposite to the wind vector. The vector of the displacement is computed by the wind vector and the time elapsed during consumption of the excess altitude. If the time for the approach can be estimated the moved position of the target configuration can be calculated. Fortunately, for co-rotating Dubins curves it is possible to give a pretty precise estimate of the approach time. Thus, we can easily calculate a wind-aware solution by moving the target configuration opposite to the wind. For the moved target, we can proceed to determine the Dubins' paths like in the windless case. Note that this approach can be applied only to path planning methods as long as there is an estimation for the glide time. In order to obtain a trajectory in the earth frame (the earth path) we can just transform the wind frame solution (the air path) by moving sampling points alongside the wind vector for the corresponding time expired since the start of the approach.

The remaining paper is organized as follows. In Section 2 we give an overview of the related work. In the third section we introduce the three dimensional Dubins curves in the windless case and how the final approach is adopted to minimize the altitude difference at the runway's threshold to a few meters above ground. Section 4 is dedicated to the description of the wind-aware extension of the Dubins curves. Afterwards, in Section 5 our simulation results for the LSLS and RSRS Dubins approaches are examined and evaluated. In the last section, we conclude the proposed results and give an outlook on our future work.

2 Related work

During the past decades, the calculation of flight paths under emergency conditions has proven as a non-trivial problem. Researchers have developed several approaches to determine an optimal flight path with various kinds of targets and conditions.

These include genetic algorithms like proposed in [5] which is focused on the avoidance of cylindrical obstacles in the horizontal plane without the consideration of the influence of wind. Thereby, a random- and an elitism-based immigrant scheme is combined adaptively. Liu et al. proposed another genetic algorithm that is capable to determine a three-dimensional flight path under the assumption of no wind [6]. The developed algorithm is basically inspired by the biological immune system and is able to avoid obstacles.

Moreover, various swarm based algorithms are applied to enable path planning for dynamic models which includes the specialized utilization in flight path planning for an aircraft. In [7] a representative swarm algorithm is proposed which enables three-dimensional path planning for unmanned aerial vehicles (UAVs). This algorithm is capable to avoid obstacles. Unfortunately, this approach doesn't consider the influence of wind during the flight path computations. But this is crucial, especially for light weighted UAVs.

The Rapidly-exploring Random Tree (RRT) method for motion planning was introduced in 1998 by LaValle [8]. Since then, this concept of path planning was often applied to various dynamic vehicle models like robots as proposed by Pepy et al. [9]. Levora et al. introduced an informed RRT algorithm which is focused on the two-dimensional motion planning for non-linear, non-holonomic systems with an unknown inverse kinematic description [10]. However, these approaches as well as the presented genetic algorithms omit the path planning under wind impact.

Furthermore, the flight path planning is considered as a higher-dimensional optimal control problem. Adler et al. proposed an algorithm based on motion primitives which enables the calculation of a six-dimensional optimal control problem. This approach results in an energy efficient solution and reduces the planning problem to a graph-search problem under the restricted conditions of calm air [11].

Another key technique in the flight path planning field are the Dubins curves. This method was introduced by Lester E. Dubins in 1957 and has become an essential research area in the field of path planning [2]. It is mainly focused on the calculation of the shortest two-dimensional path to reach a certain target. First, the Dubins curves were applied for path planning of cars. Later, the car was exchanged by an aircraft and the technique was adopted with the goal to support three-dimensional path planning [12]. In [13] a standard autopilot with low-level controller based on Dubins curves was developed. The main objective was to maintain the aircraft undamaged during the flight instead of reaching a certain target within minimum distance or flight time.

Unfortunately, this new technique still neglects the influence of wind. Nevertheless, the consideration of the wind effect is a crucial issue. Hence, Warren and Coombes et al. investigate the flight path planning problem influenced by wind in [14] and in [15]. The circle-pattern of the Dubins curves is replaced by a trochoid pattern. In the earth frame a constant wind causes a distortion of circles flown in the wind frame to a so called trochoids. Schopferer et al. have introduced a quite similar approach based on the Dubins curves and the trochoid pattern. This algorithm combines the Dubins curves algorithm used for the calculation of the flight path in the horizontal plane with a bang-bang control strategy to facilitate three-dimensional flight path planning in a constant wind [16]. Izuta et al. have presented a flight path planning algorithm to adjust the length of the final approach with the goal to improve the reachability in a forced landing. Unfortunately, they assume the windless case and if they increase or decrease the final approach, changes in the length of the flight path during both turns are left unconsidered [17]. This may be interesting in the case of two contrary rotating circles.

A fixed final approach for the flight path planning was examined by Coombes et al. [15] and was further refined in the PhD thesis of Coombes [4]. The improved technique takes a constant wind into account.

Moreover, McGee et al. describe an optimal path planning algorithm in a constant wind based on the Minimum Principle. The used algorithm re-expresses the influence of the wind as the problem of finding the optimal path planning from an initial position and orientation with no wind to a final position and orientation of a moving virtual target. However, the objective of the developed algorithm was the planning of a flight path with a minimum length [18].

We propose a novel, computational efficient method based on Dubins curves to facilitate a three-dimensional flight path planning in constant wind. This approach takes the contribution of the wind into account by performing the calculations in the wind frame. Thus, the transformation into the earth frame and the complex fitting of a straight line segment between two trochoids can be avoided.

In contrast to the Dubins curves the intention of our technique is to reach the landing field at an appropriate altitude by adjusting the length of the final approach.

3 Dubins curves for emergency landings without wind

The Dubins curves were initially developed for two-dimensional path planning for car models with the objective to reach a target from a starting position within the shortest path. This path planning approach consists of the three motion primitives listed in Table 1.

Table 1: The three motion primitives and their meaning.

Symbol	**Description**
S	Straight ahead
R	Closest possible turn to the right
L	Closest possible turn to the left

Dubins has demonstrated that a combination of only three motion primitives is necessary to calculate the shortest path between two car configurations [2]. Besides, Dubins showed that only six concatenations of the introduced motion primitives result in a possible optima. In Fig. 1 the following four configurations are illustrated.

$$\{\text{LSL, RSR, LSR, RSL}\}$$

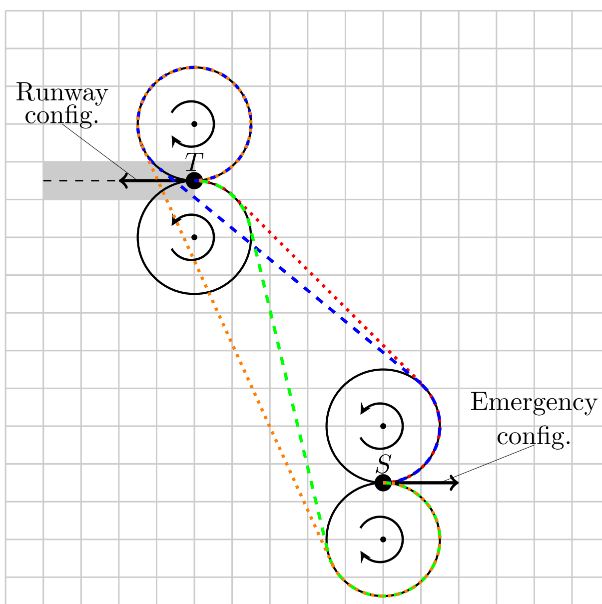

Figure 1: Considered flight path opportunities to reach the runway from a certain position.

Therein, the previously mentioned motion primitives for the four flight paths are shown. The point S denotes the start position and the arrow attached to S is the heading of the aircraft. Furthermore, the runway is illustrated as gray rectangle in the top on the left-hand side. The corresponding direction of the runway is denoted by the arrow attached to our target point (runway threshold) T.

In the present work, we consider an approach which is composed of two tangents and two co-rotating circular segments. Depending on the rotation of the circular segments, the approaches are called LSLS (two left rotating circles) and RSRS (two right rotating circles). The other approaches are left for future work.

3.1 Three-dimensional path planning

The considered car model was replaced by an aircraft model to facilitate three-dimensional path planning. The configuration of the aircraft can be expressed as $c = (x, y, z, \psi, \phi, \theta)$, where the vector (x, y, z) describes the three-dimensional position, ψ represents the heading, ϕ the bank angle, and θ the pitch angle.

First, the turning radius is calculated using Eq. 1, where r is the radius of the initial and the final turn, V_a denotes the speed of the aircraft, g represents the gravitational acceleration (9.80665 $\frac{m}{s^2}$), and ϕ is the bank angle that can differ in the sign [12].

$$r = \frac{V_a^2}{g \cdot tan(\phi)} \tag{1}$$

The pilot has to fly the turn with bank angle ϕ to realize the radius r. For simplification purposes the turnings are considered as circles as shown in Fig. 1. The outer and inner tangents (dotted and dashed straight line segments) are fitted to the four circles [12]. The inner tangents are computed for the RSLS and the LSRS approach. The outer tangents are calculated for the LSLS and the RSRS approach. Only four tangents in combination with the turnings can facilitate the desired final heading of the aircraft.

3.2 Direct calculation of co-rotating circle approaches

This subsection shows how an approach path can be calculated directly for two cases without the necessity of an iterative procedure. The following parameters are required as input for the algorithm: coordinates and heading of the aircraft and the runway, the elevation difference between aircraft and runway, the radius of both circles, the optimal speeds in curve and straight-ahead flight and the corresponding glide ratios in the straight-ahead and curve segments. The glide ratio indicates the amount of altitude an aircraft loses on a predetermined distance. For example, a glide ratio of 0.1 indicates that an aircraft loses 1 meter of altitude by gliding a distance of 10 meters. The environmental parameters are wind velocity and direction.

3.2.1 Preliminary work

To simplify the calculation, some preparatory work has to be done. First, the coordinates (latitude, longitude) of the runway and the aircraft are transformed from the geographical coordinate system into a Cartesian coordinate system. After the conversion, the origin of the Cartesian coordinate system denotes the target point of the approach path.

In the next step, the coordinate system is rotated around the origin such that the approach direction of the runway is in the direction of the positive x-axis. We also need to pay attention that the heading of the aircraft and the direction of the wind vector must be likewise rotated. Since a runway has two approach directions, we perform the following calculations for both of them. For the right side approach we implement the calculation and can compute paths for any start configuration. For the left side approach, we rotate the coordinate system by 180° and perform the same calculation applied to the right side approach. Afterwards, the computed path has to be rotated back. The basic computation is identically for both sides as presented in the following.

3.2.2 Initial configuration and summary of cases

The initial situation after the rotation can be seen in Fig. 2. The point S denotes the converted and rotated aircraft starting position of the path. The point T is the target and is located in the origin of the coordinate system. By assuming windless environmental conditions, the point T corresponds to the destination point in the wind as well as the earth frame. Otherwise, the point T is moved towards the wind direction with the magnitude of the wind vector over the approximated approach time t_a as described in Sec. 4. The calculation of the co-rotating circle approach is the same in both cases. The initial heading of the aircraft is represented by a black arrow. The approach direction of the runway is aligned to the positive x-axis. In addition to that, the co-rotating approach paths are shown with left-turning circle segments – solid – and right-turning circle segments – dotted – which are located on the start-circles I_1, I_2 and end-circles O_1, O_2.

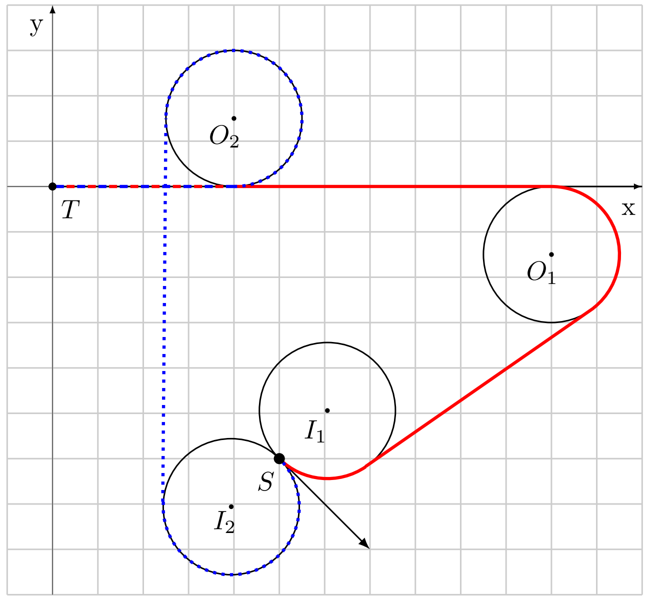

Figure 2: Schematic approach paths for LSLS and RSRS approaches.

The next step is to summarize some cases like shown in Fig. 3. A RSRS approach with starting point (x_0, y_0) corresponds to the LSLS approach with starting point $(x_0, -y_0)$, mirrored at the x-axis. This procedure is also valid for the reversed case. The current considered RSRS approach with the starting point S is mirrored at the x-axis. Thus, the following calculation can be considered as an LSLS approach with the starting point S'. Finally, the computed path has to be mirrored back. In the same way, the calculation can be done for the other side of the runway. In this case the start configuration of the aircraft is mirrored at the y-axis. In the further work we show the calculation of the LSLS approach from the right side. The LSLS approach from the left side and the RSRS approaches from right and left side of the origin can be derived from LSLS right approach by mirroring as previously explained.

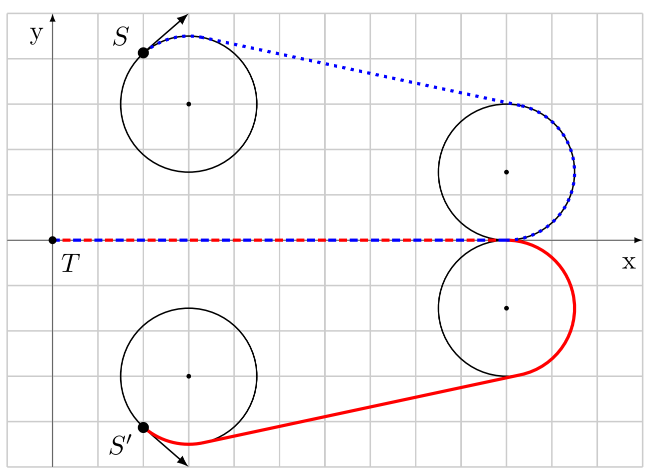

Figure 3: Mirroring at the x-axis and converting from RSRS-approach to LSLS-approach.

3.2.3 Approach calculation

The initial configuration is shown in Fig. 4 as an example for a LSLS approach. The path is subdivided into four segments: an in-segment d_I, a tangent-segment d_T, an out-segment d_O and an end-segment d_E. For a RSRS approach, the partitioning is similar.

The coordinates of the start-circle are calculated with the heading of the aircraft ψ and the given radius r of the circle. The point (x_1, y_1) is located on the left-side orthogonal to the heading direction of the aircraft with distance r. In the case of a right turning in-circle, the point on the right-side orthogonal to ψ with distance r is determined.

For a left-turning out-circle, the y-value equals $-r$, so that the circle touches the x-axis from below. For a right-turning out-circle the y-value is r so that the circle touches the y-axis from above.

The distance between the origin and the out-circle in x-direction – in the following denoted by d_E – can be varied to adjust the length of the final approach. Thus, the difference in altitude between the aircraft and the runway can be reduced. The different glide ratios in turning s_C and straight flight segments s must be considered as shown in Eq. 2.

$$\Delta_H = (d_T + d_E) \cdot s + (d_I + d_O) \cdot s_C \quad . \tag{2}$$

The total altitude difference between starting and target configuration Δ_H, corresponds to the sum of the reduced altitudes in the four segments. Thereby, d_E can be calculated directly from this equation.

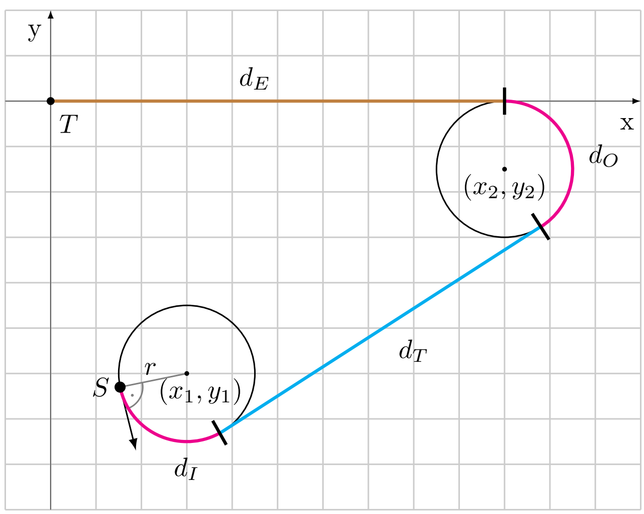

Figure 4: Approach segmentation for the LSLS approach.

If the circle segments rotate in the same direction, the sum of the segments $(d_I + d_O)$ can be derived from the total flown angle β and the radius r. Thereby, β is calculated from the aircraft heading ψ and the runway direction (here 270°). For an LSLS approach with $90° \leq \psi < 270°$ the value is $\beta = 90° + \psi$. A case distinction has to be performed for a start configuration between $270° \leq \psi < 90°$. If d_E is negative or so large that the out-circle is too far on the right side of the runway threshold right an additional rotation of 360° has to be executed. The total covered angle sums up to $\beta = 360° + 90° + \psi$. For a RSRS approach the same applies with slightly difference. In this case the angle is located at the other direction from the heading but β can be calculated.

For a known angle β, the sum of the circular segments d_C is computed as shown in Eq. 3.

$$d_C = d_I + d_O = 2 \cdot r \cdot \pi \cdot \frac{\beta}{360°} \quad . \tag{3}$$

Afterwards, the length of the tangent segment d_T is a function of d_E as described by Eq. 4.

$$d_T = \sqrt{(y_2 - y_1)^2 + (d_E - x_1)^2} \quad . \tag{4}$$

Subsequently, Eq. 3 and 4 are substituted in Eq. 2. This results in Eq. 5.

$$\Delta_H = \sqrt{(y_2 - y_1)^2 + (d_E - x_1)^2} \cdot s + d_E \cdot s + d_C \cdot s_C \quad . \tag{5}$$

Finally, Eq. 5 is solved for d_E which is shown in Eq. 6.

$$d_E = \frac{-\Delta_H^2 + (s \cdot x_1)^2 + 2 \cdot \Delta_H \cdot d_C \cdot s_C - (d_C \cdot s_C)^2 + (s \cdot y_1)^2 - 2 \cdot s^2 \cdot y_1 \cdot y_2 + (s \cdot y_2)^2}{2 \cdot s \cdot (-\Delta_H + s \cdot x_1 + d_C \cdot s_C)} \quad . \tag{6}$$

Using Eq. 6, the final approach length d_E of the end-circle can be precisely calculated. The resulting approach reduces the altitude of the aircraft accurately. Note that d_E should be positive, otherwise the length of the approach path is too long for the available altitude of the aircraft and the runway is not reachable. A value of 0 implies that the approach can still be flown with the current altitude but the end-circle touches the target point. Furthermore, the case distinction regarding to the calculation of β can lead to certain altitudes which cannot be eliminated. In this case, it may be possible that the extended approach becomes too long. A solution of this problem includes other alternative approach paths, e. g. an RSLS or an LSRS approach. By combining these approaches it is ensured that at least one valid approach path is obtained from a certain minimum altitude.

4 Wind-aware extension of Dubins curves

As an airplane moves in the wind, we usually only observe its resulting trajectory on the ground in the earth frame. It is caused by the vector addition of the momentary speeds of the aircraft and the wind which is assumed to be constant. The influence of the wind has to be taken into account, if the wind speed reaches a significant amount of the aircrafts true air speed.

4.1 Trochoids in earth frame

In order to determine an approach path influenced by a constant wind vector, mainly the earth frame has been used so far. The procedure is based on so-called trochoids, which represent the orbit of a circular flight in the earth frame at a constant wind. Thereby, a trochoid is applied to the start and end configuration of a path. Afterwards, a tangent that connects these two trochoids is adapted. In Fig. 5 we see an illustration of the method proposed by [4].

If the two trochoids are connected by the tangent, the amount of altitude reduction during the glide can be determined. If the remaining altitude at the end position is still too high for a safe flatten out on the runway, the parameters of the approach have to be adjusted. For example, the start trochoid could be left after the second, third or even a higher number of turns. Analogously, one can start the entry into the end trochoid with a higher number of cycles. In Fig. 5 a tangent is shown for one or two rotations at the start and end trochoid (dotted and dashed line).

While these parameters only effect discrete changes in height, a fine adjustment of the flatten out height can only take place by the adaptation of the trochoids' radii. As one can easily see the possibilities for the adaptation of the altitude loss are manifold and it is difficult to find the proper combination of those parameters in a short period of time. Besides, the calculation and application of new trochoids, a new tangent between those two trochoids has to be updated for each change in the parameters.

4.2 Dubins curves with moved target in wind frame

In the following, we propose an approach that can be applied to consider the influence of wind in the context of Dubins curves or any other path planning methods. As already mentioned, the central idea is to transform from earth frame to wind frame. By moving the target configuration contrary to the position where it is moved by the wind, we can perform the calculations for the path planning in the same manner as in the windless case.

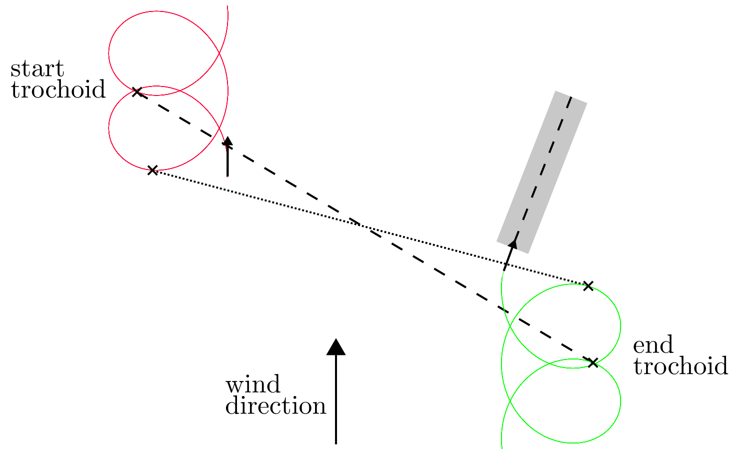

Figure 5: Trochoids in earth frame.

Fig. 6 illustrates the principle of *moving target*. Here, the target is moved into the wind for the time t_a and a usual Dubins-based LSRS approach is conducted. Note that we consider the trajectory in the wind frame which moves along the wind vector over the earth frame. Thus, this air path in the wind frame remains unchanged and the wind's influence will be modeled just by the moved target.

In order to determine the displacement for the target we have to know the time t_a for the approach. Fortunately, this time can be calculated directly for the LSLS and RSRS Dubins curves. The turns have the same direction and the corresponding turn angels β_S and β_E sum up to the total flown angle β. With this result and the glide ratio s_C we can compute the altitude loss during the turns as

$$\Delta h_C = d_C \cdot s_C \quad . \tag{7}$$

This altitude has to be subtracted from the available altitude Δ_H in order to obtain the altitude remaining for the straight portion d_S of the flight path which yields

$$d_S = (\Delta_H - \Delta h_C) \cdot s \quad . \tag{8}$$

Finally, with Eq. 3 and Eq. 8 and the corresponding aircraft velocities v_C and v_S we obtain the time t_a for moving the target from T_S to T_E as presented in Fig. 6:

$$t_a = \frac{d_C}{v_C} + \frac{d_S}{v_S} \quad . \tag{9}$$

At the time of emergency, the target point of the path is located at T_S. It has to be moved towards the wind by $t_a \cdot v_W$ to the moved target position T_E, where v_W denotes the wind velocity. The direction of the movement is given to the opposite of the wind vector's direction that is denoted by Φ_W.

4.3 Approximation of t_a for LSRS and RSLS

For the LSRS or RSLS Dubins curves the approach time t_a cannot be computed directly, because the turns have opposite directions. The time t_a depends on the (opposite directed) circular turns β_S and β_E for which we determine the complete approach, see Fig. 6.

We have to know the target configuration which itself can only be determined by the approach time.

In the following, we briefly sketch how to proceed. To start the calculation we have to compute an extended LSRS or RSLS Dubins curve from the starting point S to T_S. The total time t_0 for this (windless) approach can be used as the first estimate for t_a, denoted by $\hat{t_a}$ in the following. The

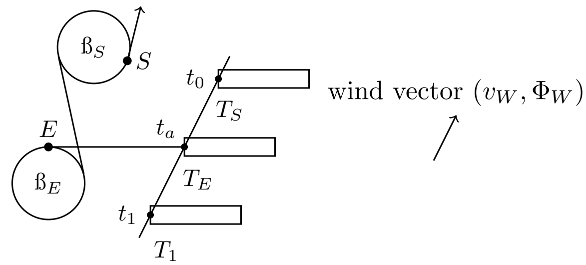

Figure 6: Modified LSRS Dubins curve in the wind frame.

time t_0 is computed as shown in equation Eq. 9. In contrast to the LSLS/RSRS case we have to compute the complete approach before the circular turn portion d_C is known.

Because the initial estimate t_0 is for the windless case, we have to increase it by a constant factor greater then 1 in order to get a new moved target for the approach time estimate t_1 in the wind-aware case. With t_1 we create a new target T_1 as described above, recompute the Dubins curve and evaluate the resulting approach time $\hat{t_a}$. If $\hat{t_a}$ is sufficiently close to t_1 we obtained the required estimate for t_a. Otherwise, we have to tweak t_1 further towards the estimate. If the approach time $\hat{t_a}$ was greater than t_1 we did move the target to much towards the wind and get t_2 by multiplying t_1 with a factor less than 1. In this way, we can create a sequence of estimations t_i until we obtain an acceptable estimation for the approach time t_a.

In order to obtain the flight path in the earth frame one can easily transform the wind frame solution by moving sampling points alongside the wind vector for the corresponding time elapsed since the start of the approach.

5 Results

In our previous research [19] we have covered the theoretical part of the flight path calculation. In the present study we propose our results obtained by a configurable simulator which covers a closed solution for the co-rotating approaches (RSRS, LSLS). The developed simulator is also capable to sweep the whole sample space for possible flight paths between the strobed starting and the fixed target configuration (runway threshold). To achieve comprehensive results, we need to provide reasonable step sizes and bounds to our simulation software for the following parameter:

- X and Y grid extent (in m),
- initial aircraft altitude (in m) and heading (in degree), and
- wind velocity (in $\frac{km}{h}$) and direction (in degree).

The beforehand listed items are parametrized as shown in Table 2.

Table 2: Hodograph independent values.

Parameter	**From**	**To**	**Step size**
Grid extend X $[m]$	$-5\,000$	$5\,000$	100
Grid extend Y $[m]$	$-5\,000$	$5\,000$	100
Initial aircraft altitude $[m]$	50	4000	10
Initial aircraft heading $[°]$	0	315	45
Wind velocity $\left[\frac{km}{h}\right]$	0	100	10
Wind direction $[°]$	0	315	45

Note that the examined grid has an extend in longitude and latitude (x, y) direction of $10\,000\,m$ respectively. The horizontal plane of our grid is sampled with a step size of $100\,m$. Furthermore, it can be seen from Table 2 that the initial altitude of the aircraft varies from $50\,m$ to $4\,000\,m$ above the runway which is assumed to be on sea-level. The altitude is stepped with a resolution of $10\,m$. It is obvious that the altitude is finer sampled as the extend in the horizontal plain because the variation of the altitude has a greater influence on the results. Moreover, the wind velocity is sampled by a step size of $10\,\frac{km}{h}$ within a range from $0\,\frac{km}{h}$ to $100\,\frac{km}{h}$. Ultimately, the coarse scanning of the solution space regarding to the wind direction is also shown in Table 2.

Furthermore, we need to provide the following aircraft model specific parameter to our simulation software:

- Aircraft velocity on straight flight segment and during turnings ($\frac{km}{h}$),
- glide ratio on straight flight segment and during turnings, and
- radius (m).

We selected a Cessna 182 in the present study, because this aircraft is widely used and well known in General Aviation (GA). It was possible to acquire some research results of [4] regarding to the velocity hodographs which are shown in Fig. 7.

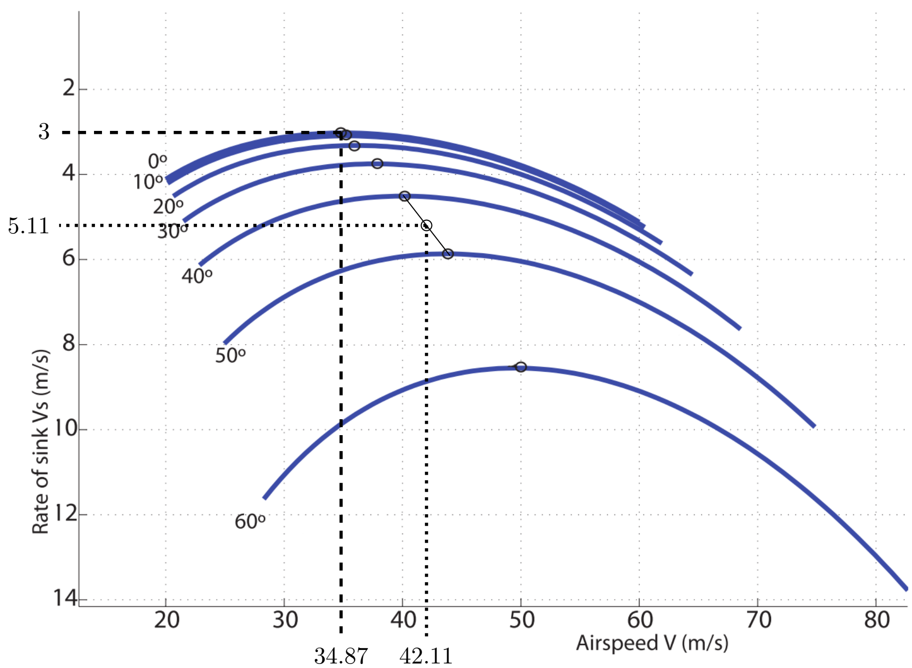

Figure 7: Hodographs of a Cessna 182 for various bank angles [4].

Thereby, the aircraft velocity ($\frac{m}{s}$) is plotted against the rate of sink ($\frac{m}{s}$). Each curve – illustrated as solid lines – in Fig. 7 represents the hodograph relating to the corresponding bank angle which is labeled on the left side at the beginning of each graph. The points – marked with circles – denote the aircraft velocity with minimum sink rate at the particular bank angle.

For the parametrization of our simulation, the rate of sink V_s and the velocity of the aircraft V_a with minimum sink rate for the straight flight and during the turnings have to be determined. These values are obtained from the previously mentioned hodographs. We selected a bank angle of 15° and 45°. The bank angle of 45° is stated as optimal bank angle for a glide through a 190° to 220° heading change – regarding to the minimum altitude loss during the turning flight – in [20] and [4]. For that reason, we assume this value as a comprehensive parametrization opportunity for the bank angle. In [21] the optimal bank angle peaked to a value of 65° for a F-16 fighter aircraft model. It is also mentioned that the turn-back trajectories for a Cessna Skyhawk 172 (GA) is similar and it is assumed that the same applies to other GA-Models like the chosen Cessna 182. However, such an extreme value for the bank angle is considered as too dangerous for the chosen aircraft model. To make assertions about the influence of the bank angle change, we also examine a bank angle of 15°.

The technique to obtain the desired values for V_s and V_a is shown in Fig. 7 for straight flight – dashed lines – and turnings with a bank angle of 45° – dotted lines. The data for a bank angle of 45° is estimated by a linear regression. We also obtain the values for a bank angle of 15° with the same procedure.

Based on the preserved data, the prior listed parameters are determined. They are shown in Table 3 for a bank angle of 15° and 45°.

Table 3: Hodograph dependent values for bank angle 15° and 45°.

Parameter	**Bank angle** 15°	**Bank angle** 45°
Aircraft velocity straight flight $\left[\frac{km}{h}\right]$	125.53	125.53
Aircraft velocity in turning flight $\left[\frac{km}{h}\right]$	128.84	151.6
Glide ratio straight flight	0.086	0.086
Glide ratio in turning flight	0.089	0.121
Radius $[m]$	487.47	180.82

Note that the aircraft velocity with a minimum rate of sink grows with an increase of the bank angle. In addition, the glide performance decreases with the rise of the bank angle. This becomes especially obvious by considering the glide ratio. For straight flight, we obtain a glide ratio of 0.086 which means that the aircraft losses $0.86\,m$ in altitude by travelling $10\,m$ above ground. The drop of altitude by a bank angle of 15° increases slightly to an amount of $0.89\,m$. The altitude loss by a bank angle of 45° adds up to $1.21\,m$. Hence, the difference in the reduction of altitude per $10\,m$ travelled over ground between a bank angle of 15° and 45° reach a total of $0.32\,m$ which can be expressed as an increase of 35.96 %. Thus, as a result of the earlier indicated behavior of the gliding properties regarding to the bank angle, the radius depends on the bank angle. The greater the bank angle is, the smaller will the radius during the turning flights be. Thereby, the radius is computed by solving Eq. 1.

A total of about 11 billion path calculations were executed by the simulator (2.8 billion start configurations with each four paths – LSLS-left, LSLS-right RSRS-left and RSRS-right). The total duration of the calculation was 5 hours 16 minutes achieved by a modern Desktop-PC (Intel i7 7700K, 32 GB RAM) which corresponds to $1.67\,\mu s$ per path planning computation. The results are summarized in Table 4. At least one valid path was found for about 2.4 billion start configurations. These corresponds to 85 % of all the start configurations and shows that a large number of paths can be found with co-rotating circles. Considering cross rotating circles, this number should increase even further. No path could be found for about 250.4 million start configurations because the flight altitude was too low even in direct gliding flight to the runway. In this case, the pilot will never be able to reach the runway independently from the path type. For the remaining start configurations the altitude would be high enough for straight glide but the runway cannot be reached by adding further turns.

Table 4: Results of the simulation with 15° bank angle.

Duration of calculation $[s]$	19 007.913
Start settings	2 843 875 584
Path calculations	11 375 502 336
Start settings with too low altitude	250 417 216
Start settings with min. one valid path	2 440 262 708
Start settings with exact one valid path	146 736 824
Start settings with min. two valid paths	2 293 525 884
Start settings with min. two opposite paths	2 241 931 714

This circumstance is represented in Fig. 8. In the following a fixed start configuration is considered with a varying altitude and only one possible path type. Each configuration can be either of type a) or of type b). In the most cases a configuration is of type a), so that above a minimum altitude (Min.) every altitude can be reduced with a valid flight path (represented by the solid black line) as shown in Fig. 8 a). In some cases, the range of the possible altitudes with valid paths is discontinuously, Fig. 8 b). This occur at the transitions between two different case distinctions, such as the flight of an additional full circle. Then, certain altitudes cannot be reduced by a valid path until the altitude is high enough for an additional full turn. Consequentially, the range of correct reducible altitudes has a gap as shown in Fig. 8 b). This problem can be avoided if other path types are considered. Than a valid path for each altitude above the minimum altitude can be calculated and every configuration is of type a). It is worthwhile that the number of start configurations with more than one valid path is as large as possible.

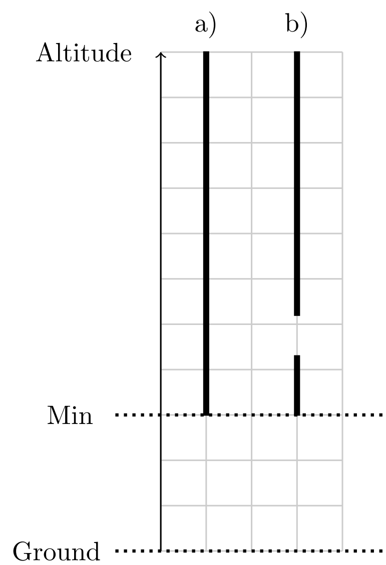

Figure 8: Altitudes with valid approaches.

Of all start configurations there were about 146.7 million with exactly one and about 2.3 billion with more than one path, see Table 4. In the second case, several possible approach paths can be selected. This is particularly important when it comes to the inclusion of obstacles or other requirements for the path.

For the start configurations with more than one valid path, about 2.2 billion configurations contained at least two opposite approaches, i.e. either LSLS-left/LSLS-right, RSRS-left/RSRS-right or all four approaches. In these cases, the better direction depending on the wind can be selected which makes it easier for the pilot to land.

In a second run, the calculations were repeated for a bank angle of 45°, see Table 5. The increased angle changes the optimum speeds, sliding conditions and the radius of the circles, see Table 3. A curve with 45° bank angle is assumed to be hard to fly for an aircraft as well as for the pilot. Nevertheless, in an emergency situation this extreme bank angle should be considered as possible. When comparing Table 4 and Table 5, it is noticeable that the number of start configurations with at least one path found increases. This result was expected because the reduced curve radius decreases the total approach distance, which means that a lower altitude is sufficient to calculate a valid path. The number of configurations that does not reach the runway even in straight flight (too low altitude) remained the same, since the radius of the circle has no influence on this number.

At 45° bank angles, more configurations with at least two paths and two opposite paths are found. This was expected because the smaller radius increases the number of possible paths.

Some more configurations are possible which were infeasible with 15° and other configurations are removed because they have more than one valid path with 45°. In this run, there was a reduction from about 146.7 to 64.1 million starting configurations with exact one path. Further investigations could be made if a larger bank angle would generally find fewer configurations with exactly one path.

Table 5: Results of the simulation with 45° bank angle.

Duration of calculation [s]	18 722.378
Start settings	2 843 875 584
Path calculations	11 375 502 336
Start settings with too low altitude	250 417 216
Start settings with min. one valid path	2 515 845 172
Start settings with exact one valid path	64 177 796
Start settings with min. two valid paths	2 451 667 376
Start settings with min. two opposite paths	2 432 399 502

6 Conclusion and future work

In this paper we presented solutions for an emergency landing assistant based on modified Dubins curves that model the properties of turn and straight flight and extend it to three-dimensional space. We also propose a new approach to take the wind offset into consideration. Compared to trochoid approaches the proposed method avoids complex computations for fitting the tangents between the two trochoids and can be applied to any approach path.

We have developed and tested a simulator for automatic flight path calculations. In total, we have calculated approximately 11.4 billion paths for nearly 2.8 billion start configurations and analyzed the results according to several criteria. We extended the basics of path calculations and present the results of the simulation. For 85% of all start configurations, we found valid flight paths with co-rotating circles approaches. This number should increase even further by implementing the RSLS and LSRS approaches.

In future work we will focus on the RSLS and LSRS Dubins curves and implement the sketched procedure to estimate the approach time for moving the target in the presence of wind. Moreover, we are going to apply AI methods to create a database of emergency landings fields based on public available geodata.

References

[1] F. Eckstein, B. Wittich, and W. Schiffmann, "Emergency landing field recognition based on elevation data using parallel processing," in *Proceedings of the Digital Avionics Systems Conference* (AIAA, ed.), 2018.

[2] L. E. Dubins, "On Curves of Minimal Length with a Constraint on Average Curvature, and with Prescribed Initial and Terminal Positions and Tangents," *American Journal of Mathematics*, vol. 79, pp. 497–516, 1957.

[3] M. Owen, R. W. Beard, and T. W. McLain, "Implementing dubins airplane paths on fixed-wing uavs," *Handbook of Unmanned Aerial Vehicles*, pp. 1677–1701, 2015.

[4] M. Coombes, *"Landing site reachability and decision making for UAS forced landings Making for UAS Forced Landings"*. PhD thesis, Loughborough University, 2016.

[5] X. Fu and X. Gao, "Genetic algorithm with adaptive immigrants for dynamic flight path planning," in *2010 IEEE Int. Con. on Intelligent Computing and Intelligent Systems*, vol. 1, pp. 630–634, Oct 2010.

[6] L. Liu and S. Zhang, "Three-dimensional flight path planning by artificial immune algorithm," *Natural Computation, 6th Int. Conf.*, pp. 2876–2880, 2010.

[7] Y. Cai, H. Zhao, M. Li, and H. Huang, "3D real-time path planning based on cognitive behavior optimization algorithm for UAV with TLP model," in *Cluster Computing*, 2018.

[8] S. M. Lavalle, "Rapidly-exploring random trees: A new tool for path planning," 1998.

[9] R. Pepy, A. Lambert, and H. Mounier, "Path Planning using a Dynamic Vehicle Model," *2006 2nd Int. Conf. on Information and Communication Technologies*, vol. 1, 2006.

[10] T. Levora, O. Bruna, and P. Pavel, "Path planning for ultralights under emergency," in *29th Congress of the International Council of the Aeronautical Sciences*, (St. Petersburg, Russia), pp. 1–7, 2014.

[11] A. Adler, A. Bar-Gill, and N. Shimkin, "Optimal flight path for engine-out emergency landing," in *24th Control and Decision Conference*, IEEE, 2012.

[12] P. Eng, L. Mejias, X. Liu, and R. Walker, "Automating human thought processes for a UAV forced landing," *Journal of Intelligent and Robotic Systems: Theory and Applications*, vol. 57, no. 1-4, pp. 329–349, 2010.

[13] P. Donato and E. Atkins, "Three-dimensional dubins path generation and following for a uas glider," in *Int. Con. on Unmanned Aircraft Systems*, pp. 294–303, June 2017.

[14] M. Warren, L. Mejias, J. Kok, X. Yang, F. Gonzalez, and B. Upcroft, "An automated emergency landing system for fixed-wing aircraft: Planning and control," *Journal of Field Robotics*, vol. 32, no. 8, pp. 1114–1140, 2015.

[15] M. Coombes, W.-H. Chen, and P. Render, "Reachability Analysis of Landing Sites for Forced Landing of a UAS in Wind using Trochoidal Turn Paths," *Journal of Intelligent and Robotic Systems*, vol. 73, no. 1-4, pp. 635–653, 2015.

[16] S. Schopferer and T. Pfeifer, "Performance-aware flight path planning for unmanned aircraft in uniform wind fields," *Int. Conf. on Unmanned Aircraft Systems*, pp. 1138–1147, 2015.

[17] S. Izuta and M. Takahashi, "Path Planning to Improve Reachability in a Forced Landing," *Journal of Intelligent and Robotic Systems*, vol. 86, no. 2, pp. 291–307, 2017.

[18] T. McGee, S. Spry, and J. Hedrick, "Optimal path planning in a constant wind with a bounded turning rate," *AIAA Guidance, Navigation, and Control Conference*, pp. 1–11, 2005.

[19] M. Klein, A. Klos, J. Lenhardt, and W. Schiffmann, "Wind-aware Emergency Landing Assistant Based on Dubins Curves," in *The 5th Int. Symp. on Computing and Networking*, (Aomori, Japan), pp. 1–5, 2017.

[20] D. F. Rogers, "The Possible Impossible Turn," in *AIAA Journal of Aircraft*, vol. 32, pp. 392–397, 1995.

[21] K. Brinkman and H. G. Visser, "Optimal turn-back manoeuvre after engine failure in a single-engine aircraft during climb-out," in *Journal of Aerospace Engineering*, vol. 221, pp. 17–27, 2007.

Appendix

Notation

Symbol	**Meaning**
d_C	Length of circle segments
d_E	Length of end approach
d_S	Length of line segments
d_T	Length of tangent segment
g	Gravitational acceleration (9.80665 $\frac{m}{s^2}$)
I	In-cirle center
O	Out-cirle center
r	Turning radius
S	Approach start point
s	Glide ratio straight-ahead
s_C	Glide ratio in curves
T	Approach end point
t_a	Time of approach
V_a	Aircraft speed indicated
β	Total flown angle
Δ_H	Initial Altitude difference between aircraft and runway
Δh_C	Loss of altitude in circle segments
ϕ	Bank angle
Φ_W	Opposite of the wind vector's direction